



## Article

# Gain-Scheduled Control Design Applied to Classical dc–dc Converters in Photovoltaic Systems and Constant Power Loads

Roberto M. Fuentes <sup>1</sup>, Jonathan M. Palma <sup>1,\*</sup>, Hildo Guillard Junior <sup>2</sup>, Márcio J. Lacerda <sup>3</sup>,  
Leonardo de P. Carvalho <sup>4</sup>, Alejandro J. Rojas <sup>5</sup> and Ricardo C. L. F. Oliveira <sup>6</sup>

<sup>1</sup> Faculty of Engineering, University of Talca, Curicó 3340000, Chile

<sup>2</sup> School of Engineering of São João da Boa Vista, São Paulo State University—UNESP, São João da Boa Vista 15054-000, SP, Brazil

<sup>3</sup> Control and Modelling Group (GCOM), Department of Electrical Engineering, Federal University of São João del-Rei—UFSJ, São João del-Rei 36307-352, MG, Brazil

<sup>4</sup> Polytechnic School, Telecommunications Engineering and Control Department, University of São Paulo—USP, São Paulo 05508-060, SP, Brazil

<sup>5</sup> Department of Electrical Engineering, Universidad de Concepción, Concepción 4030000, Chile

<sup>6</sup> School of Electrical and Computing Engineering, University of Campinas—UNICAMP, Campinas 13083-852, SP, Brazil

\* Correspondence: jonathan.palma@utalca.cl

**Abstract:** This paper investigates the problem of control design for dc–dc converters, where the solution is especially suitable to address variations in the input voltage, a frequent situation in photovoltaic systems, and the problem of constant power load, where a nonlinear load is connected to the output of the converter. The proposed approach models the converters in terms of Linear Parameter-Varying (LPV) models, which are used to compute gain-scheduled robust gains. The synthesis conditions provide stabilizing controllers with an attenuation level of disturbances in terms of the  $\mathcal{H}_\infty$  norm. Moreover, the design conditions can also overcome pole locations to comply with physical application restrictions when ensuring transient performance. The validation of the controllers is made via simulation of the classical converters (buck, boost and buck-boost), showing that the proposed method is a viable and generalized control solution that works for all three converters, with guarantees of closed-loop stability and good performance.

**Keywords:** DC–DC converter; D-stability design control; H-infinity performance; LPV modeling; robust and gain-scheduled control; state-feedback control

**MSC:** 93B36; 93B50; 93B51



**Citation:** Fuentes, R.M.; Palma, J.M.; Júnior, H.G.; Lacerda, M.J.; Carvalho, L.d.P.; Rojas, A.J.; Oliveira, R.C.L.F. Gain-Scheduled Control Design Applied to Classical dc–dc Converters in Photovoltaic Systems and Constant Power Loads.

*Mathematics* **2022**, *10*, 3467. <https://doi.org/10.3390/math10193467>

Academic Editor: Cristiano Maria Verrelli

Received: 2 August 2022

Accepted: 19 September 2022

Published: 23 September 2022

**Publisher's Note:** MDPI stays neutral with regard to jurisdictional claims in published maps and institutional affiliations.



**Copyright:** © 2022 by the authors. Licensee MDPI, Basel, Switzerland. This article is an open access article distributed under the terms and conditions of the Creative Commons Attribution (CC BY) license (<https://creativecommons.org/licenses/by/4.0/>).

## 1. Introduction

The design of power converters has drawn a lot of attention in the last decades. The main reason for this fact is that power converters are used in several current technological trends, such as electrical cars, unmanned aircraft and smart grids [1–3]. These applications, on the other hand, impose some additional challenges such as efficient energy acquisition, management of renewable sources and standardization [4]. Therefore, the design of controllers for such converters is not an easy task, since several energy sources may be used at the same time [5]. Moreover, there are energy sources that can be time-varying, introducing additional complexities into the design.

Power converters are devices that allow the transformation of the electrical energy by changing its characteristics. There are several topologies of power converters, differentiated by their operating input/output voltage (ac or dc) and their applications [6,7]. These converters may present nominal values variations due to differences in the components used in their construction [8] or due to aging, in case of the capacitors [9,10], contributing

to the variation of the parameters associated to the converters. In this work, we are interested in dc–dc converters, where the classical topologies are: buck, boost and buck-boost converters [11].

When converters are implemented, depending on the application, they can present the behavior of parameter-varying systems. For example: (i) In PhotoVoltaic (PV) applications, the partial shading problem generates an operation range for the input voltage [12], instead of a fixed unique input voltage. This phenomenon affects the input of the converter. (ii) When a constant non-linear load is connected (constant power load, current constant load, active resistive load, etc.) [13,14] to the output of the converter, the system acquires load-dependent dynamics. This requires a multi-equilibrium point approach. The control design strategy proposed in this paper is especially suitable to address these two particular scenarios.

Power converters are typically controlled by classical strategies [15] such as PID control, the preferred choice for industrial applications [16]. However, simple control strategies may provide poor performance in multi-equilibrium point situations [17]. For this case, more appropriate control strategies may be: sliding mode control, fuzzy control and Model Predictive Control (MPC) [18]. Particularly, in the context of systems affected by time-varying parameters, a robust control technique that has gained notorious attention is the one based on Linear Matrix Inequalities (LMIs) [19]. Synthesis conditions based on LMIs can be solved efficiently by polynomial-time algorithms [20]. Moreover, the design procedure can easily incorporate performance criteria based on the  $\mathcal{H}_\infty$  and  $\mathcal{H}_2$  norms and  $\mathcal{D}$ -stability [21–23]. The contribution of this paper is a strategy for designing robust and gain-scheduled control applied to dc–dc converters in photovoltaic applications. The approach includes the modeling of the converter, yielding a suitable linear parameter-varying (LPV) model, which can be used to compute gain-scheduled robust gains using LMI conditions. The synthesis conditions provide stabilizing controllers with an attenuation level of disturbances in terms of the  $\mathcal{H}_\infty$  norm. Moreover, under the assumption of slow variations of the parameters, the design conditions can also provide desired pole locations to assure transient performance ( $\mathcal{D}$ -stability). The proposed methodology is tested in two simulation cases for a PV application.

The paper is organized as follows: Section 2 provides the LMI framework for the design of the controller; Section 3 presents the equilibrium point model and its LPV representation for three classical topologies of dc–dc converters; Section 4 presents a summary of the proposed methodology; Sections 5 and 6 provide simulation cases for two applications. Section 7 concludes the article.

## 2. Mathematical Framework

Notation: The set of natural numbers is denoted by  $\mathbb{N}$  and the  $n$ -th dimensional Euclidean space is expressed by  $\mathbb{R}^n$  with the usual norm  $\|\cdot\|$ . The set of real matrices with dimension  $n \times m$  is denoted by  $\mathbb{R}^{n \times m}$ . The symbol  $'$  indicates the transposition of a matrix or a vector. The symbol  $\star$  represents a block induced by symmetry in a symmetric matrix.

Consider the continuous-time linear parameter-varying (LPV) system

$$\mathcal{G} : \begin{cases} \frac{dx(t)}{dt} = A(\theta(t))x(t) + B(\theta(t))u(t) + J(\theta(t))w(t), \\ z(t) = C_z(\theta(t))x(t) + D_z(\theta(t))u(t) + E_z(\theta(t))w(t), \end{cases} \quad (1)$$

where  $x \in \mathbb{R}^{n_x}$ ,  $u \in \mathbb{R}^{n_u}$ ,  $w \in \mathbb{R}^{n_w}$ ,  $z \in \mathbb{R}^{n_z}$  are, respectively, the vector of states, control inputs, exogenous inputs and outputs. All system matrices have appropriate dimensions and are structured in the form

$$X(\theta(t)) = X_0 + \sum_{i=1}^M X_i \left( \prod_{j=1}^V \theta_j(t)^{\lambda_j^i} \right), \quad (2)$$

where  $\theta(t)$  is a vector of bounded time-varying parameters belonging to the set

$$\Theta = \{(\theta_1, \dots, \theta_V) \in \mathbb{R}^V : \underline{\theta}_j \leq \theta_j \leq \bar{\theta}_j, j = 1, \dots, V\} \tag{3}$$

for all  $t \geq 0$  and  $\underline{\theta}_j$  and  $\bar{\theta}_j$  are known values. In the most general case, the matrices of the system can depend polynomially on the time-varying parameters with  $M$  monomials and  $\lambda^i \in \mathbb{N}^V$  defining the exponents of the  $i$ -th monomial, whose associated coefficient is the matrix  $X_i$ . If  $M = V$  and  $\lambda^i = [0, \dots, 1, \dots, 0]$ , where the number 1 is at the  $i$ -th position,  $i = 1, \dots, V$ , then  $X(\theta(t))$  is a time-varying matrix with the well-known *affine* structure. Regarding the variation rate of the time-varying parameters  $\theta(t)$  over time, no hypothesis is assumed, that is, they can vary arbitrarily fast.

Assuming that  $\theta(t)$  can be measured or estimated in real time, we consider the gain-scheduled state-feedback control law  $u(t) = K(\theta(t))x(t)$  for system (1), which provides the following closed-loop dynamics

$$\mathcal{G}_K : \begin{cases} \frac{dx(t)}{dt} = (A(\theta(t)) + B(\theta(t))K(\theta(t)))x(t) + J(\theta(t))w(t), \\ z(t) = (C_z(\theta(t)) + D_z(\theta(t))K(\theta(t)))x(t) + E_z(\theta(t))w(t). \end{cases} \tag{4}$$

A standard performance criterion for the closed-loop system (4) is the  $\mathcal{H}_\infty$  norm (also known as the  $\mathcal{L}_2$  gain), defined as

$$\|\mathcal{G}_K\|_\infty = \sup_{w \neq 0} \frac{\|z\|}{\|w\|} \tag{5}$$

The next lemma presents sufficient conditions in terms of parameter-dependent LMIs to design the gain-scheduled controller  $K(\theta(t))$  assuring robust stability and an upper bound on the  $\mathcal{H}_\infty$  norm of the closed-loop system  $\mathcal{G}_K$ .

**Lemma 1** ([19]). *Let  $\mu$  be a given positive real number. If there exists a symmetric definite positive matrix  $P \in \mathbb{R}^{n_x \times n_x}$  and matrix  $Z(\theta) \in \mathbb{R}^{n_u \times n_x}$  such that the following parameter-dependent LMIs hold*

$$\begin{bmatrix} A(\theta)P + PA(\theta)' + B(\theta)Z(\theta) + Z(\theta)'B(\theta)' & J(\theta) & PC_z(\theta)' + Z(\theta)'D_z(\theta)' \\ & \star & -I & E_z(\theta)' \\ & \star & \star & -\gamma I \end{bmatrix} < 0, \tag{6}$$

$$\begin{bmatrix} P & Z(\theta)' \\ Z(\theta) & \mu I \end{bmatrix} < 0. \tag{7}$$

then the state-feedback gain  $K(\theta) = Z(\theta)P^{-1}$  robustly stabilizes system (4) and  $\|\mathcal{G}_K\|_\infty < \sqrt{\gamma}$ , that is,  $\sqrt{\gamma}$  is an  $\mathcal{H}_\infty$  guaranteed cost (upper bound) for the closed-loop system. Moreover, condition (6) assures that  $\|u\|_2^2 < \mu$  for  $x(0) = 0$ .

Pole location is a widely used criterion for robust control of linear systems, especially to assure performance criteria related to the transient behavior and respect the physical limits of the used components. Although the system under investigation is time-varying, where the notion of poles is not defined, the employment of a performance criterion based on the location of the poles can be meaningful if the system operates with slow variations of the time-varying parameters. The next lemma presents parameter-dependent LMI conditions to enforce that the closed-loop system, for frozen values of  $\theta(t)$ , has poles lying inside the region depicted in Figure 1 represented by  $\mathbb{S}(\alpha, r, d)$ , where the parameters  $\alpha, r, d \in \mathbb{R}^+$  satisfy: (i)  $a < -d < 0$ , (ii)  $|a \pm bj| < r$  and (iii)  $b < \cot(\alpha)a$ .

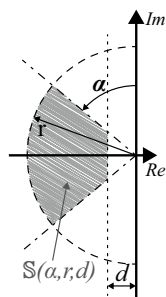


Figure 1. Region desired  $S(\alpha, r, d)$  on complex plane.

**Lemma 2.** Let  $\alpha, r, d \in \mathbb{R}^+$  be given values. If there exists a symmetric definite positive matrix  $P \in \mathbb{R}^{n_x \times n_x}$  and matrix  $Z(\theta) \in \mathbb{R}^{n_u \times n_x}$  such that the following parameter-dependent LMIs hold

$$A(\theta)P + PA(\theta)' + B(\theta)Z(\theta) + Z(\theta)'B(\theta)' + 2dP < 0, \tag{8}$$

$$\begin{bmatrix} -rP & PA(\theta)' + Z(\theta)'B(\theta)' \\ \star & -rP \end{bmatrix} < 0, \tag{9}$$

$$\begin{bmatrix} \cos(\alpha) \left( A(\theta)P + PA(\theta)' + B(\theta)Z(\theta) + Z(\theta)'B(\theta)' \right) & \sin(\alpha) \left( A(\theta)P - PA(\theta)' + B(\theta)Z(\theta) - Z(\theta)'B(\theta)' \right) \\ \sin(\alpha) \left( -A(\theta)P + PA(\theta)' - B(\theta)Z(\theta) + Z(\theta)'B(\theta)' \right) & \cos(\alpha) \left( A(\theta)P + PA(\theta)' + B(\theta)Z(\theta) + Z(\theta)'B(\theta)' \right) \end{bmatrix} < 0, \tag{10}$$

then the state-feedback gain  $K(\theta) = Z(\theta)P^{-1}$  is robustly stabilizing. Moreover, according to the *D*-stability theorem [24], for frozen values of  $\theta$ , the closed-loop poles belong to the region  $S(\alpha, r, d)$  in Figure 1.

The proofs of the presented lemmas can be found, for instance, in [19,25,26]. The conditions of both Lemmas 1 and 2 are solved simultaneously in the problem investigated in the next sections, assuring robust stability, disturbance rejection ( $\mathcal{H}_\infty$  norm), suitable transient behavior (pole in Figure 1 locations) and control signal with limited energy.

### 3. DC-DC Converter Models

DC-DC converters are well-studied systems [27,28], and their operation is based on the switching of a semiconductor device, causing the storage or discharging of energy from an inductor.

The classical topologies are shown in Figure 2, where *S* is a semiconductor switch, *D* corresponds to a diode,  $L(t)$  is the inductance value,  $C(t)$  and  $C_{in}(t)$  are the capacitance values, and  $R(t)$  denotes the load resistor value.  $d_1$  and  $d_2$  are visual guides for the direction of the current  $i_L(t)$  as a function of the operating state of *S* (by the transistor or by the diode). Finally,  $i_L(t)$  is the inductor current,  $V_{in}(t)$  is the input voltage, and  $V_{out}(t)$  is the capacitor voltage (output voltage).

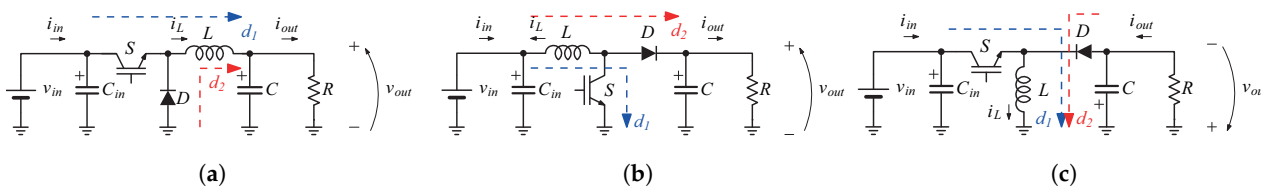


Figure 2. Topologies of three classical dc-dc converters. To improve the readability, the time-dependent parameters ( $V_{in}(t)$ ,  $C(t)$ ,  $L(t)$ ,  $i_{out}(t)$ ,  $v_{out}(t)$  and  $R(t)$ ) appear without ( $t$ ) notation. (a); Buck converter. (b) Boost converter. (c) Buck-Boost converter.

The differential equations of these converters are widely studied. The authors of [29] presented the mathematical models for multiphase schemes. For the particular case of a single phase, the differential equations are as follows:

$$\text{Buck} : \begin{cases} \frac{di_L(t)}{dt} = \frac{1}{L(t)} \left( V_{in}(t)S_{sw}(t) - v_{out}(t) \right), \\ \frac{dv_{out}(t)}{dt} = \frac{1}{C(t)} \left( i_L(t) - \frac{v_{out}(t)}{R(t)} \right). \end{cases} \tag{11}$$

$$\text{Boost} : \begin{cases} \frac{di_L(t)}{dt} = \frac{1}{L(t)} \left( V_{in}(t) - v_{out}(t) \left( 1 - S_{sw}(t) \right) \right), \\ \frac{dv_{out}(t)}{dt} = \frac{1}{C(t)} \left( i_L(t) \left( 1 - S_{sw}(t) \right) - \frac{v_{out}(t)}{R(t)} \right). \end{cases} \tag{12}$$

$$\text{Buck-Boost} : \begin{cases} \frac{di_L(t)}{dt} = \frac{1}{L(t)} \left( V_{in}(t)S_{sw}(t) - v_{out}(t) \left( 1 - S_{sw}(t) \right) \right), \\ \frac{dv_{out}(t)}{dt} = \frac{1}{C(t)} \left( i_L(t) \left( 1 - S_{sw}(t) \right) - \frac{v_{out}(t)}{R(t)} \right). \end{cases} \tag{13}$$

In the set of equations from (11) to (13),  $S_{sw}(t)$  represents the switching function. This function is usually a Pulse-Width Modulation (PWM) function or equivalent [30].

### 3.1. Small-Signal Average Model

The equilibrium point model of each converter, presented in this section, can be obtained from [31,32]. The small-signal method establishes that the converters can be represented in state-space based on deviation variables (represented by the  $\tilde{(\cdot)}$  notation) and their operation point, such as  $\frac{d\tilde{x}}{dt} = A(x_{op}, u_{op})\tilde{x}(t) + B(x_{op}, u_{op})\tilde{u}(t)$ . If we consider that the parameters are time-varying, we obtain

$$\frac{d\tilde{x}(t)}{dt} = \overbrace{\left( A_{on}(t)D_{on}(t) + A_{off}(t)D_{off}(t) \right)}^{A(x_{op}(t), u_{op}(t))} \tilde{x}(t) + \overbrace{\left( B_{on}(t)D_{on}(t) + B_{off}(t)D_{off}(t) \right)}^{B(x_{op}(t), u_{op}(t))} \tilde{u}(t), \tag{14}$$

where  $A_{on}(t)$  and  $B_{on}(t)$  indicate the model when  $S$  is closed (operative, based on the  $S_{sw}(t)$  function), while  $A_{off}(t)$  and  $B_{off}(t)$  denote the model when  $S$  is open (does not conduct current),  $D_{on}(t)$  is the conduction time of the switch at the point of operation and  $D_{off}(t)$  is its complement, such that  $D_{on}(t) + D_{off}(t) = 1$ , as continuous mode operation of the converters [33]. The new state vector  $\tilde{x}(t)$  is a deviation of the state signals with respect to the operation point,  $\tilde{u}(t)$  is an input variation with respect to operation input. Thus, the small-signal average models are given by

$$\text{Buck}_{ssa} : \begin{cases} \frac{d\tilde{x}(t)}{dt} = \begin{bmatrix} 0 & -\frac{1}{L(t)} \\ \frac{1}{C(t)} & -\frac{1}{R(t)C(t)} \end{bmatrix} \tilde{x}(t) + \begin{bmatrix} \frac{V_{in}(t)}{L(t)} \\ 0 \end{bmatrix} \tilde{u}(t), \end{cases} \tag{15}$$

$$\text{Boost}_{ssa} : \begin{cases} \frac{d\tilde{x}(t)}{dt} = \begin{bmatrix} 0 & -\frac{D_{off}(t)}{L(t)} \\ \frac{D_{off}(t)}{C(t)} & -\frac{1}{R(t)C(t)} \end{bmatrix} \tilde{x}(t) + \begin{bmatrix} \frac{V_{in}(t)}{D_{off}(t)L(t)} \\ -\frac{V_{in}(t)}{C(t)R(t)D_{off}^2(t)} \end{bmatrix} \tilde{u}(t), \end{cases} \tag{16}$$

$$\text{Buck-Boost}_{ssa} : \begin{cases} \frac{d\tilde{x}(t)}{dt} = \begin{bmatrix} 0 & -\frac{D_{off}(t)}{L(t)} \\ \frac{D_{off}(t)}{C(t)} & -\frac{1}{R(t)C(t)} \end{bmatrix} \tilde{x}(t) + \begin{bmatrix} \frac{V_{in}(t)}{D_{off}(t)L(t)} \\ \frac{V_{in}D_{on}(t)}{C(t)R(t)D_{off}^2(t)} \end{bmatrix} \tilde{u}(t). \end{cases} \tag{17}$$

The models given in (15)–(17) can be rewritten in a nonlinear affine form as shown below

Buck in nonlinear affine form:

$$\frac{d\tilde{x}(t)}{dt} = \left( \begin{bmatrix} 0 & -1 \\ 0 & 0 \end{bmatrix} \frac{1}{L(t)} + \begin{bmatrix} 0 & 0 \\ 1 & 0 \end{bmatrix} \frac{1}{C(t)} + \begin{bmatrix} 0 & 0 \\ 0 & -1 \end{bmatrix} \frac{1}{R(t)C(t)} \right) \tilde{x}(t) + \left( \begin{bmatrix} 1 \\ 0 \end{bmatrix} \frac{V_{in}(t)}{L(t)} \right) \tilde{u}(t), \tag{18}$$

Boost in nonlinear affine form:

$$\begin{aligned} \frac{d\tilde{x}(t)}{dt} = & \left( \begin{bmatrix} 0 & -1 \\ 0 & 0 \end{bmatrix} \frac{D_{off}(t)}{L(t)} + \begin{bmatrix} 0 & 0 \\ 1 & 0 \end{bmatrix} \frac{D_{off}(t)}{C(t)} + \begin{bmatrix} 0 & 0 \\ 0 & -1 \end{bmatrix} \frac{1}{R(t)C(t)} \right) \tilde{x}(t) \\ & + \left( \begin{bmatrix} 1 \\ 0 \end{bmatrix} \frac{V_{in}(t)}{D_{off}(t)L(t)} + \begin{bmatrix} 0 \\ 1 \end{bmatrix} \frac{V_{in}(t)}{C(t)R(t)D_{off}^2(t)} \right) \tilde{u}(t), \end{aligned} \tag{19}$$

Buck-Boost in nonlinear affine form:

$$\begin{aligned} \frac{d\tilde{x}(t)}{dt} = & \left( \begin{bmatrix} 0 & -1 \\ 0 & 0 \end{bmatrix} \frac{D_{off}(t)}{L(t)} + \begin{bmatrix} 0 & 0 \\ 1 & 0 \end{bmatrix} \frac{D_{off}(t)}{C(t)} + \begin{bmatrix} 0 & 0 \\ 0 & -1 \end{bmatrix} \frac{1}{R(t)C(t)} \right) \tilde{x}(t) \\ & + \left( \begin{bmatrix} 1 \\ 0 \end{bmatrix} \frac{V_{in}(t)}{D_{off}(t)L(t)} + \begin{bmatrix} 0 \\ -1 \end{bmatrix} \frac{V_{in}(t)D_{on}(t)}{C(t)R(t)D_{off}^2(t)} \right) \tilde{u}(t). \end{aligned} \tag{20}$$

### 3.2. Parameter-Dependent dc–dc Converters Control Design

The classical control design for a dc–dc converter is based on tracking a given set-point. The set-point tracking is made defining a new state  $x_e(t)$ , which maps a single reference with error criterion defined by

$$x_e(t) = \int_0^\tau (V_{ref} - v_{out}(t))dt, \tag{21}$$

where  $x_e(t)$  is the tracking reference error (more details can be found in [34] (Section 2) and/or [35] (Section 2)). The new state represents the dynamic equation  $\frac{dx_e}{dt} = V_{ref} - v_{out}(t)$  that, combined with the states of the converter, yields an augmented system of  $n + 1$  states given by,

$$\begin{aligned} \frac{dx(t)}{dt} &= \left[ \begin{array}{c|c} A_g(t) & \begin{bmatrix} 0 \\ 0 \end{bmatrix} \\ \hline \begin{bmatrix} 0 & -1 \end{bmatrix} & 0 \end{array} \right] x(t) + \left[ \begin{array}{c} B_g(t) \\ 0 \end{array} \right] u(t) + \left[ \begin{array}{c} J_g(t) \\ 0 \end{array} \right] w(t) + \begin{bmatrix} 0 \\ 0 \\ 1 \end{bmatrix} V_{ref}, \\ z(t) &= \begin{bmatrix} 0 & 1 & 0 \end{bmatrix} x(t), \end{aligned} \tag{22}$$

where  $x(t) = [\tilde{x}(t)' \ x_e(t)']'$ ,  $u(t) = \tilde{u}(t)$ , and  $z(t) = v_{out}(t)$ . The matrices  $A_g(\theta(t))$  and  $B_g(\theta(t))$  can be replaced by the matrices associated with the converters represented by (15)–(17). The dynamics presented in (18)–(20) are a particular case of (1) with null matrix  $J(\theta(t))$ , however, (with further analysis) it can be shown that the variation of the load current ( $\tilde{i}_{load}$ ) represents a higher/lower current demand, which can be considered as an external input to the system, being suitably represented as the matrix  $J_g(\theta(t))$  with disturbance vector given by  $w(t) = \tilde{i}_{load}(t)$ . Regarding system (1), matrices  $D_z(\theta(t))$  and  $E_z(\theta(t))$  are null. Note that  $[0 \ 0 \ 1]' \cdot V_{ref}$  is a concept introduced for reference tracking purposes. For control, it is not considered in the design where the reference is constant (see [34,35]).

We assume that the parameters  $C(t)$ ,  $L(t)$ ,  $D_{on}(t)$ ,  $R(t)$  and  $V_{in}(t)$  are time-varying and bounded. To generate an LPV model with matrices structured as in (2), the following change of variables is adopted:  $\theta_1(t) = 1/L(t)$ ,  $\theta_2(t) = 1/C(t)$ ,  $\theta_3(t) = 1/R(t)$ ,  $\theta_4(t) = D_{off}(t)$ ,  $\theta_5(t) = 1/\theta_4(t)$  and  $\theta_6(t) = V_{in}(t)$ . Notice that to eliminate the rational dependency on  $\theta_4$ ,

not admissible by the model, the parameter  $\theta_5$  has been included, possibly introducing some conservatism. If we define the matrices,

$$A_0 = \begin{bmatrix} 0 & 0 & 0 \\ 0 & 0 & 0 \\ 0 & -1 & 0 \end{bmatrix}, A_1 = \begin{bmatrix} 0 & -1 & 0 \\ 0 & 0 & 0 \\ 0 & 0 & 0 \end{bmatrix}, A_2 = \begin{bmatrix} 0 & 0 & 0 \\ 1 & 0 & 0 \\ 0 & 0 & 0 \end{bmatrix}, A_3 = \begin{bmatrix} 0 & 0 & 0 \\ 0 & -1 & 0 \\ 0 & 0 & 0 \end{bmatrix},$$

$$B_0 = \begin{bmatrix} 1 \\ 0 \\ 0 \end{bmatrix}, B_1 = \begin{bmatrix} 0 \\ -1 \\ 0 \end{bmatrix}, B_2 = \begin{bmatrix} 0 \\ 1 \\ 0 \end{bmatrix}, J_0 = \begin{bmatrix} 0 \\ -1 \\ 0 \end{bmatrix},$$

the LPV models with polynomial dependency on the parameters given in (23)–(25) are obtained.

Buck linear parameter-dependent model:

$$\frac{dx(t)}{dt} = (A_0 + A_1\theta_1(t) + A_2\theta_2(t) + A_3\theta_2(t)\theta_3(t))x(t) + B_0\theta_1(t)\theta_6(t)u(t) + J_0\theta_2(t)w(t) \quad (23)$$

Boost parameter-dependent model:

$$\frac{dx(t)}{dt} = (A_0 + A_1\theta_1(t)\theta_4(t) + A_2\theta_2(t)\theta_4(t) + A_3\theta_2(t)\theta_3(t))x(t) + (B_0\theta_1(t)\theta_5(t)\theta_6(t) - B_1\theta_1(t)\theta_3(t)\theta_5(t)^2\theta_6(t))u(t) + J_0\theta_2(t)w(t) \quad (24)$$

Buck-Boost parameter-dependent model:

$$\frac{dx(t)}{dt} = (A_0 + A_1\theta_1(t)\theta_5(t) + A_2\theta_2(t)\theta_5(t) + A_3\theta_2(t)\theta_3(t))x(t) + (B_0\theta_1(t)\theta_5(t)\theta_6(t) + B_2\theta_2(t)\theta_3(t)\theta_5(t)^2\theta_6(t)(1 - \theta_4(t)))\tilde{u}(t) + J_0\theta_2(t)w(t) \quad (25)$$

where  $u(t) = [\tilde{d}(t)]$  is the control variable,  $x(t) = [\tilde{i}_L(t) \quad \tilde{v}_{out}(t) \quad x_e(t)]'$  is the state vector and  $w(t) = [\tilde{i}_{load}(t)]$  is the modeled perturbation. The terms associated to  $x(t)$ ,  $u(t)$  and  $w(t)$  represent, respectively, the system's dynamics matrix  $A(\theta(t))$ , the control input matrix  $B(\theta(t))$  and the exogenous input matrix  $J(\theta(t))$ .

#### 4. Proposed Control Scheme

The proposed control scheme is presented in Figure 3, and it can be applied to any type of dc–dc converter. Note that the gain-scheduled state-feedback controller is obtained offline, even though the controller is updated in real-time (according to the values of scheduling parameters). To accomplish this offline step, a sequence of steps must be performed, as illustrated in Figure 4 and detailed in the following Algorithm 1:

---

##### Algorithm 1 Offline steps.

---

- 1: Obtain an LPV state-space model for the converter aimed to be controlled.
  - 2: The model must be written in the form (2) according to the pre-specified values of the bounds of the time-varying parameters  $\underline{\theta}_j$  and  $\bar{\theta}_j$ .
  - 3: The design variables are obtained based on the application.
  - 4: For given values of  $\alpha$ ,  $d$ ,  $r$  and  $\mu$ , use the conditions of Lemmas 1 and 2 to define a set of LMIs. The Robust LMI Parser (ROLMIP) can be used to perform this task [36].
  - 5: Solve the set of LMIs using a semi-definite programming (SDP) solver to obtain the set of gains of the controller and a guaranteed cost  $\gamma$  for the closed-loop system. A resume of the computational complexity can be seen in Appendix B.
-

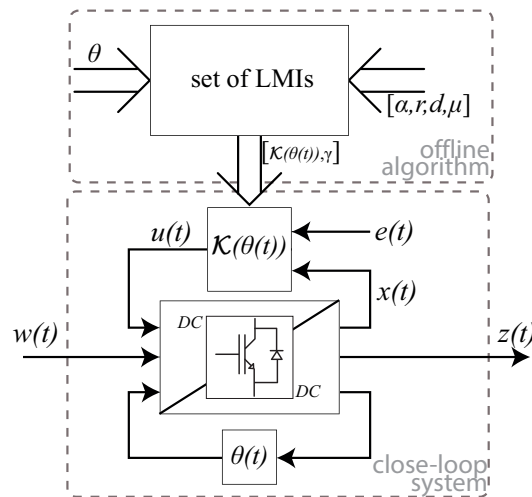


Figure 3. Scheme of design.

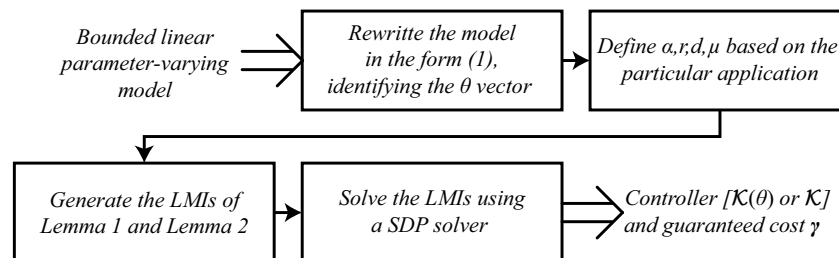


Figure 4. Offline algorithm.

### 5. Photovoltaic System Application

A converter connected to a PV panel is subject to perturbations, which can be suitably modeled in terms of a linear system affected by time-varying parameters. To optimize the performance of the control system, a gain-scheduled controller, i.e., a controller which is updated by the values of the time-varying parameters in real-time, is proposed. For the application under investigation, we considered the PV system Kyocera KC200GT (Datasheet available on (<https://www.datasheets.com/en/part-details/kc200gt-kyocera-62747508>), accessed on 2 August 2022), connected to the topologies in Figure 2. This PV panel is a solar module with an array of four serial-connected modules that, based on official meteorological data of irradiance and temperature [37], generates all the curves shown in Figure 5.

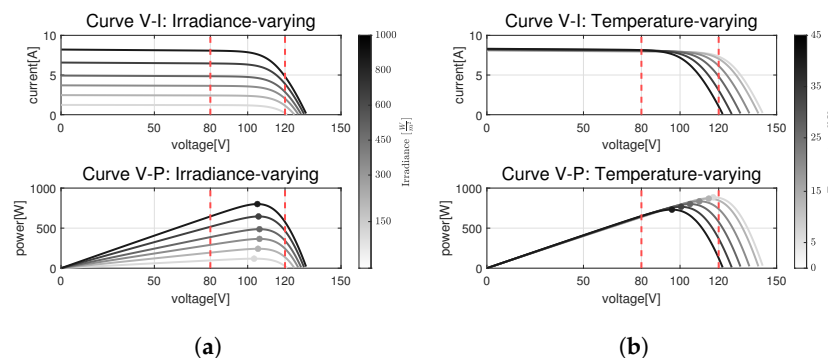


Figure 5. The points (•)(•)(•)(•)(•)(•) represent the maximum powers according to each case. (a) Irradiance curves for constant temperature of 25 °C. (b) Temperature curve for a constant irradiance of 1000 W m<sup>-2</sup>.



The results presented in this figure show all the operational ranges of the equipment, and from that, the maximum power point can be seen to be located in an input voltage range (Note that the input voltage range can be arbitrarily chosen based on the steps given in Section 5) between 80 V to 120 V. Thus, we consider  $\theta_6(t)$  to vary in this range for the synthesis of the controller.

The parameters of the PV panel used in the design are presented in Table 1a. The simulations were performed considering the nonlinear models using MATLAB/Simulink 2022b software and the toolbox *Simscape/Specialized Power Systems* [38] (more details in Appendix A).

**Table 1.** Numerical values: Photovoltaic approach.

(a) Converter parameters values		
Parameter	Value	Unit
$L$	$1 \pm 20\%$	$mH$
$C$	$680 \pm 20\%$	$\mu F$
$R$	$10 \pm 20\%$	$\Omega$
$V_{in}$	$100 \pm 20\%$	$V$
$D_{on,buck}$	[0.3 0.7]	
$D_{on,boost}$	[0.3 0.7]	
$D_{on,buck-boost}$	[0.3 0.7]	
(b) Design variables for $\mathbb{S}(\alpha, r, d)$		
Parameter	Value	Unit
$f_{sw}$	40	$kHz$
$d$	100	$s^{-1}$
$r$	$2\pi f_{sw}/20 = 1.25 \times 10^4$	$s^{-1}$
$\alpha$	$\pi/6$	$rad\ s^{-1}$
$\mu$	7	

The selected design variables for  $\mathbb{S}(\alpha, r, d)$  are shown in Table 1b. A switching frequency  $f_{sw} = 40\text{ kHz}$  was considered to assure a valid small signal linear model of the converters. Finally,  $|a + jb| \leq (2\pi f_{sw})/20\text{ rad s}^{-1}$  was considered to calculate  $r$ .

### 5.1. Synthesized Controllers

Two controllers are designed using the proposed approach. The first is a standard state-feedback gain, not scheduled by any time-varying parameter. The second one is parameter-dependent, scheduled by  $\theta_3(t)$  and  $\theta_6(t)$ , the only parameters that can be measured in real time in this application. Regarding the polynomial dependency of  $K(\theta(t))$  on these parameters, the following structure has been chosen:

$$\mathcal{K}(\theta(t)) = \mathcal{K}_0 + \mathcal{K}_3\theta_3(t) + \mathcal{K}_6\theta_6(t) \tag{26}$$

that is,  $K(\theta(t))$  is affine (degree one) on both  $\theta_3(t)$  and  $\theta_6(t)$ . Observe that the first controller (parameter-independent) is a particular case of (26) (with  $\mathcal{K}_3 = \mathcal{K}_6 = 0$ ). As a consequence, it is expected that the second controller provides better performance.

Applying the proposed control design technique considering (22) and the values informed in Table 1, one obtains the results shown in Table 2. For comparisons purposes, the controllers obtained with the technique from [26] are also designed and shown in Table 2 (to make the comparison possible, the quadratic stability conditions of [26] were extended to address LPV matrices).

**Table 2.** Controllers <sup>1</sup> synthesized with the proposed approach and the method from [26].

Converter	Gains $\mathcal{K}'$	Proposed Controllers		Bound $\gamma$		Controller [26] <sup>2</sup> Gains $\mathcal{K}'$
		Gains $\mathcal{K}(\theta(t))'$		Numerical	In dB	
Buck	$\begin{bmatrix} -0.0888 \\ -0.1709 \\ 25.0734 \end{bmatrix}$	$\begin{bmatrix} -0.19928 \\ -0.33637 \\ 55.2392 \end{bmatrix}$	$+ \theta_6(t) \begin{bmatrix} 0.00098 \\ 0.00169 \\ -0.27347 \end{bmatrix}$	0.5477	-5.229 dB	$\begin{bmatrix} -0.0167 \\ -0.0019 \\ 1.7637 \end{bmatrix}$
Boost	$\begin{bmatrix} -0.0407 \\ -0.0286 \\ 6.0457 \end{bmatrix}$	$\begin{bmatrix} -0.08644 \\ -0.07224 \\ 14.4806 \end{bmatrix}$	$+ \theta_3(t) \begin{bmatrix} -0.12550 \\ -0.10549 \\ 21.4341 \end{bmatrix} + \theta_6(t) \begin{bmatrix} 0.00048 \\ 0.00040 \\ -0.08133 \end{bmatrix}$	2.0248	6.127 dB	$\begin{bmatrix} -0.0566 \\ -0.0308 \\ 5.4237 \end{bmatrix}$
Buck-Boost	$\begin{bmatrix} -0.0245 \\ -0.0401 \\ 6.0796 \end{bmatrix}$	$\begin{bmatrix} -0.06431 \\ -0.13127 \\ 17.9773 \end{bmatrix}$	$+ \theta_3(t) \begin{bmatrix} 0.053211 \\ 0.15441 \\ -15.1723 \end{bmatrix} + \theta_6(t) \begin{bmatrix} 0.00029 \\ 0.00059 \\ -0.082358 \end{bmatrix}$	1.8708	5.440 dB	$\begin{bmatrix} -0.0113 \\ -0.0037 \\ 1.0636 \end{bmatrix}$

<sup>1</sup> For a format with more decimal digits, please refer to <https://github.com/RFuentesAlbornoz/CC-LMI/> (accessed on 1 August 2022). <sup>2</sup> This work does not consider the  $\mathcal{H}_\infty$  performance, therefore, it is not possible to obtain the  $\gamma$  values.

5.2. Performance in Terms of Tracking Errors

Table 3 is presented to compare the performance across the different controllers by computing all the index costs (based on (27)) of the tracking errors that were obtained.

$$\mathcal{J} = \int_0^\tau |v_{ref} - v_{out}(t)| dt \tag{27}$$

**Table 3.** Results of simulation in the PV example.

Converter	Index Cost				
	LTI Case		LPV Case		
	Robust Proposed	Robust [26]	Robust Proposed	G-S Proposed	Robust [26]
Buck	0.607	0.625	0.6983	0.6431	1.214
Boost	1.223	1.453	1.825	1.750	2.099
Buck-Boost	1.257	1.506	1.635	1.416	2.516

The controllers designed with the proposed approach offered better performance with respect to literature controller [26] in both the LTI and LPV cases. Among the proposed controllers, the gain-scheduled ones, as expected, provided superior performance in all three cases.

5.3. Additional Simulations

In this section, we present two additional simulations. The first simulation considers the parameters as fixed and time-invariant. The second simulation assumes the parameters to be bounded and time-varying. Figures 6 and 7 show the states of the converters working with the proposed controllers and with the controller designed with the technique from [26]. The setpoints for each converter are  $v_{ref}^{bu} = 80$  V for the buck,  $v_{ref}^{bo} = 150$  V for the boost and  $v_{ref}^{bu-bo} = 150$  V for the buck-boost converter.

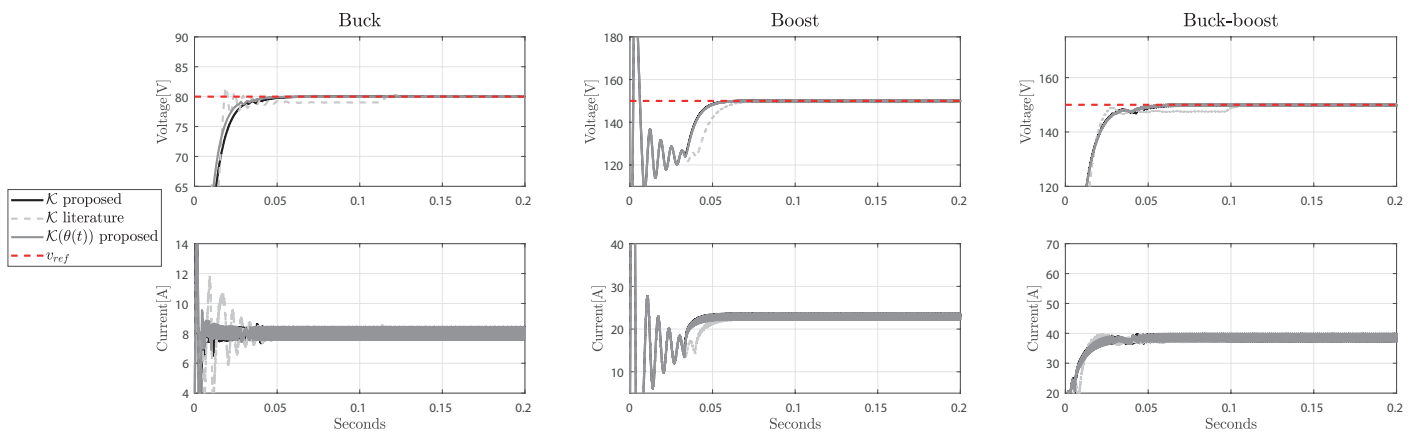


**Figure 6.** DC–DC converters state response for fixed and time-invariant parameters under PV approach, where nominal values were used for the simulations, i.e.,  $L = 1$  mH,  $C = 680$   $\mu$ F,  $R = 10$   $\Omega$ ,  $V_{in} = 100$  V and  $i_{load} = 0.5$  A. The upper figures indicate the voltage and the setpoint on the three converters. The lower figures show the current obtained in the inductor.

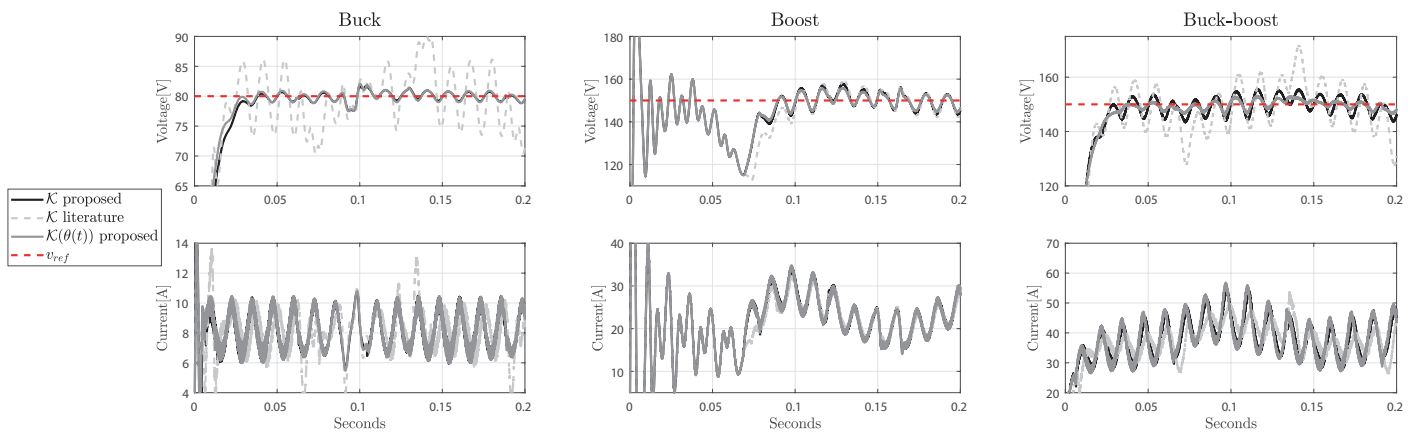


**Figure 7.** DC–DC converters state response for time-varying bounded parameters assumed to vary according to:  $R(t) = 10 + 2 \cdot \sin(500t)$   $\Omega$ ,  $i_{load}(t) = 0.5 \cdot \sin(1000t)$  A,  $L(t) = 1 + 0.2 \cdot \sin(400t)$  mH,  $C(t) = 680 + 136 \cdot \sin(300t)$   $\mu$ F and  $V_{in}(t) = 100 + 20 \cdot \sin(50t)$  V. The upper figures indicate the voltage and the setpoint on the three converters. The lower figures show the current obtained in the inductor.

Figure 7 allows to conclude that all controllers respond to parametric uncertainty variations appropriately. The major contribution to cost index occurs during the reference step.

### 6. Application to CLP Problem

In generation systems, Constant Power Load (CPL) is a phenomenon that occurs when two converters are interconnected and the fed converter has faster dynamics than the feeding one [14]. This problem is modeled assuming that the fed converter is a load to the feeding converter, as shown in Figure 8,

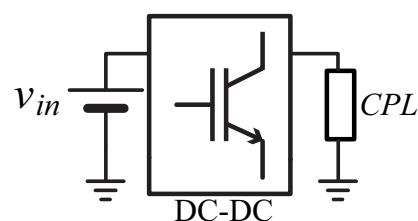


**Figure 8.** Scheme of dc-dc converter with CPL.

where the dc–dc converter can be any architecture investigated in this paper (Figure 2a–c) considering that  $R(t)$  is now a CPL device. Note that  $P(t)$  is a power demand on the fed converter and it is considered constant. This implies that the differential Equations (11)–(13) must be modified so that the  $\frac{v_{out}(t)}{R(t)}$  term is replaced by  $\frac{P(t)}{v_{out}(t)}$ , giving rise to Equations (28)–(30).

$$\text{Buck}_{CPL} : \begin{cases} \frac{di_L(t)}{dt} = \frac{1}{L(t)} \left( V_{in}(t) S_{sw}(t) - v_{out}(t) \right), \\ \frac{dv_{out}(t)}{dt} = \frac{1}{C(t)} \left( i_L(t) - \frac{P(t)}{v_{out}(t)} \right). \end{cases} \tag{28}$$

$$\text{Boost}_{CPL} : \begin{cases} \frac{di_L(t)}{dt} = \frac{1}{L(t)} \left( V_{in}(t) - v_{out}(t) (1 - S_{sw}(t)) \right), \\ \frac{dv_{out}(t)}{dt} = \frac{1}{C(t)} \left( i_L(t) (1 - S_{sw}(t)) - \frac{P(t)}{v_{out}(t)} \right). \end{cases} \tag{29}$$

$$\text{Buck-Boost}_{CPL} : \begin{cases} \frac{di_L(t)}{dt} = \frac{1}{L(t)} \left( V_{in}(t) S_{sw}(t) - v_{out}(t) (1 - S_{sw}(t)) \right), \\ \frac{dv_{out}(t)}{dt} = \frac{1}{C(t)} \left( i_L(t) (1 - S_{sw}(t)) - \frac{P(t)}{v_{out}(t)} \right). \end{cases} \tag{30}$$

It is not feasible to use the small-signal method to linearize Equations (28)–(30), therefore, we use the first-order Taylor series expansion. This method is studied in [39] and its use can be found in the literature [40,41]. The linearized systems are then:

$$\text{Buck}_{CPL} : \begin{cases} \frac{d\tilde{x}(t)}{dt} = \begin{bmatrix} 0 & -\frac{1}{L} \\ -\frac{1}{C} & \frac{P(t)}{Cv_{out}(t)^2} \end{bmatrix} \tilde{x}(t) + \begin{bmatrix} \frac{V_{in}(t)}{L} \\ -\frac{i_L(t)}{C} \end{bmatrix} \tilde{u}(t) + \begin{bmatrix} \frac{D_{on}(t)}{L} & 0 \\ 0 & -\frac{1}{Cv_{out}(t)} \end{bmatrix} \tilde{w}(t) \end{cases} \tag{31}$$

$$\text{Boost}_{CPL} : \begin{cases} \frac{d\tilde{x}(t)}{dt} = \begin{bmatrix} 0 & -\frac{(D_{on}-1)}{L} \\ -\frac{(D_{on}-1)}{C} & \frac{P(t)}{Cv_{out}(t)^2} \end{bmatrix} \tilde{x}(t) + \begin{bmatrix} \frac{v_{out}(t)}{L} \\ -\frac{i_L(t)}{C} \end{bmatrix} \tilde{u}(t) + \begin{bmatrix} \frac{1}{L} & 0 \\ 0 & -\frac{1}{Cv_{out}(t)} \end{bmatrix} \tilde{w}(t) \end{cases} \tag{32}$$

$$\text{Buck-Boost}_{CPL} : \begin{cases} \frac{d\tilde{x}(t)}{dt} = \begin{bmatrix} 0 & -\frac{(D_{on}-1)}{L} \\ -\frac{(D_{on}-1)}{C} & \frac{P(t)}{Cv_{out}(t)^2} \end{bmatrix} \tilde{x}(t) + \begin{bmatrix} \frac{V_{in}(t)+v_{out}(t)}{L} \\ -\frac{i_L(t)}{C} \end{bmatrix} \tilde{u}(t) + \begin{bmatrix} \frac{D_{on}(t)}{L} & 0 \\ 0 & -\frac{1}{Cv_{out}(t)} \end{bmatrix} \tilde{w}(t) \end{cases} \tag{33}$$

### 6.1. Linear Parameter-Dependent Model

Following the same procedure of Section 3.2, a linear augmented system with tracking-reference and parameter-dependency is obtained from (31)–(33). The vector of bounded time-varying parameters is chosen as:  $\theta_1(t) = D_{on}(t)$ ,  $\theta_2(t) = P(t)$ ,  $\theta_3(t) = 1/v_{out}(t)$ ,  $\theta_4(t) = v_{out}(t)$ ,  $\theta_5(t) = i_L(t)$  and  $\theta_6(t) = V_{in}(t)$ . Note that parameter  $\theta_4(t)$  can introduce some conservatism since the inverse of  $v_{ou}(t)$  also appears in  $\theta_3(t)$ . Defining the matrices

$$A_0 = \begin{bmatrix} 0 & -\frac{1}{L} & 0 \\ \frac{1}{C} & 0 & 0 \\ 0 & -1 & 0 \end{bmatrix}, A_1 = \begin{bmatrix} 0 & \frac{1}{L} & 0 \\ -\frac{1}{C} & 0 & 0 \\ 0 & -1 & 0 \end{bmatrix}, A_2 = \begin{bmatrix} 0 & -\frac{1}{L} & 0 \\ \frac{1}{C} & 0 & 0 \\ 0 & 0 & 0 \end{bmatrix}, A_3 = \begin{bmatrix} 0 & 0 & 0 \\ 0 & \frac{1}{C} & 0 \\ 0 & 0 & 0 \end{bmatrix},$$

$$B_0 = \begin{bmatrix} \frac{1}{L} \\ 0 \\ 0 \end{bmatrix}, B_1 = \begin{bmatrix} 0 \\ \frac{1}{C} \\ 0 \end{bmatrix}, B_2 = \begin{bmatrix} -\frac{1}{L} \\ 0 \\ 0 \end{bmatrix}, J_0 = \begin{bmatrix} \frac{1}{L} & 0 \\ 0 & 0 \\ 0 & 0 \end{bmatrix}, J_1 = \begin{bmatrix} 0 & 0 \\ 0 & -\frac{1}{C} \\ 0 & 0 \end{bmatrix},$$

the LPV models of the converters associated to the CLP approach are then given by (34)–(36).

Buck CPL parameter-dependent:

$$\frac{d\tilde{x}}{dt} = (A_0 + A_3\theta_2(t)\theta_3(t)^2)\tilde{x}(t) + (B_0\theta_6(t))\tilde{u}(t) + (J_0\theta_1(t) + J_1\theta_3(t))\tilde{w}(t), \tag{34}$$

Boost CPL parameter-dependent:

$$\frac{d\tilde{x}}{dt} = (A_1 + A_2\theta_1(t) + A_3\theta_2(t)\theta_3(t)^2)\tilde{x}(t) + (B_2\theta_4(t) + B_1\theta_5(t))\tilde{u}(t) + (J_0\theta_1(t) + J_1\theta_3(t))\tilde{w}(t), \tag{35}$$

Buck-Boost CPL parameter-dependent:

$$\frac{d\tilde{x}}{dt} = (A_1 + A_2\theta_1(t) + A_3\theta_2(t)\theta_3(t)^2)\tilde{x}(t) + (B_2\theta_4(t) + B_0\theta_6(t) + B_1\theta_5(t))\tilde{u}(t) + (J_0(\theta_1(t)) + J_1\theta_3(t))\tilde{w}(t). \tag{36}$$

### 6.2. Synthesized Controllers

For this study case, the numerical values of Table 4a and design values of Table 4b are used to synthesize the controllers.

**Table 4.** Numerical values of converters: CPL approach.

(a) Converter parameters values		
Parameter	Value	Unit
$L$	1	$mH$
$C$	100	$\mu F$
$P$	[300 500]	$W$
$V_{in}$	$100 \pm 20\%$	$V$
$D_{on,buck}$	[0.5 0.8]	
$D_{on,boost}$	[0.4 0.6]	
$D_{on,buck-boost}$	[0.4 0.6]	
(b) Design variables for $\mathbb{S}(\alpha, r, d)$		
Parameter	Value	Unit
$f_{sw}$	40	$kHz$
$d$	150	$s^{-1}$
$r$	$2\pi f_{sw}/20 = 1.25 \times 10^4$	$s^{-1}$
$\alpha$	$\pi/6$	$rad\ s^{-1}$
$\mu$	7	

By applying the proposed synthesis procedure with values suitable to the CPL approach, the controllers shown in the Table 5 were obtained. The  $\mathcal{H}_\infty$  guaranteed costs as well as the index cost (based on (27)) obtained in the simulations are also informed.

**Table 5.** Synthesized controllers.

Converter	Proposed Controllers Gains $\mathcal{K}$	Bound $\gamma$		Index Cost
		Numerical	In dB	
Buck	$[-0.1211 \quad -0.0529 \quad 9.1235]^T$	0.2090	-13.5971 dB	1.115
Boost	$[-0.0488 \quad -0.0188 \quad 4.6591]^T$	0.8871	-1.0405 dB	1.843
Buck-Boost	$[-0.0439 \quad -0.0238 \quad 5.0733]^T$	0.3040	-10.3425 dB	2.058

### 6.3. Simulations

For a representative simulation, a square signal is used as demanded power. This signal varies between its minimum and maximum each 0.1 s (significantly slower with respect to the voltage/current dynamics). The aim is to track a step-type reference at 0.25 s from 80 V to 50 V for the buck converter, and from 200 V to 150 V for both boost and buck-boost converters, while the power demand remains constant. The responses

are shown in Figures 9–11. Figure 9 shows that the converters supply the power demand for the CPL, and present approximated ripples of  $\pm 0.1$  W,  $\pm 0.2$  W and  $\pm 0.2$  W, for buck, boost and buck-boost converters, respectively. At step-changes in voltage reference  $v_{ref}$ , the power supplied presents a weak performance for a short period (0.01 s). Figure 10 and Figure 11 show the converters' states holding the voltage  $v_{out}(t)$  close to the reference  $v_{ref}$ , whilst the current compensates the changes in power demand, with its permanent variation and a ripple, respectively.

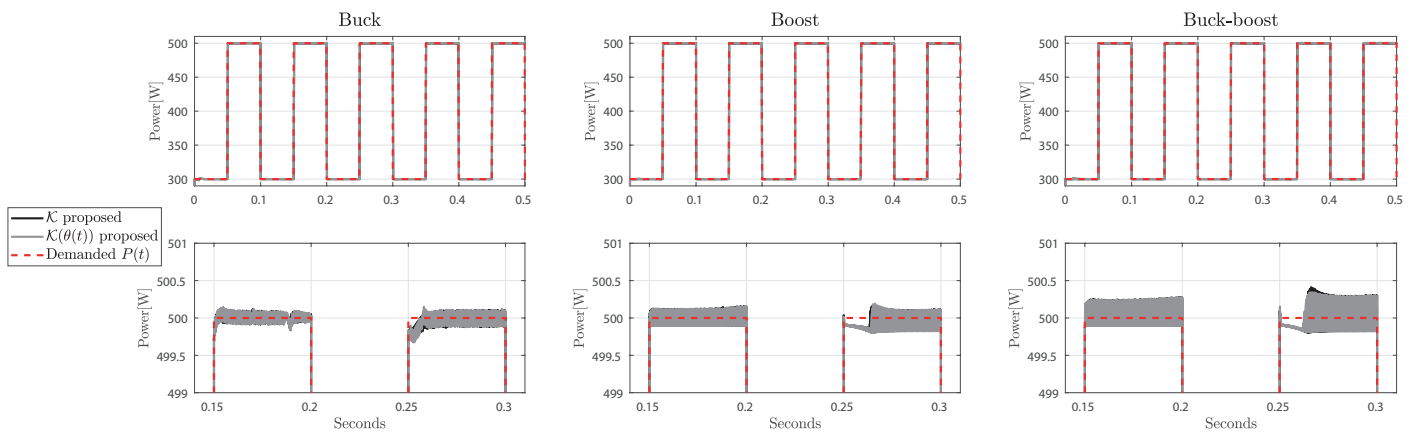


**Figure 9.** Power demand for bounded and time-varying case based on CLP problem. This case considered the nominal value for  $V_{in} = 100$  V and  $P(t)$  as a square signal with amplitude  $\in [300\ 500]$  W and frequency of 10 Hz to simulate. The upper figures indicate the given power and the power demand of the CPL. The lower figures show a zoom of the step-changes in power demand.

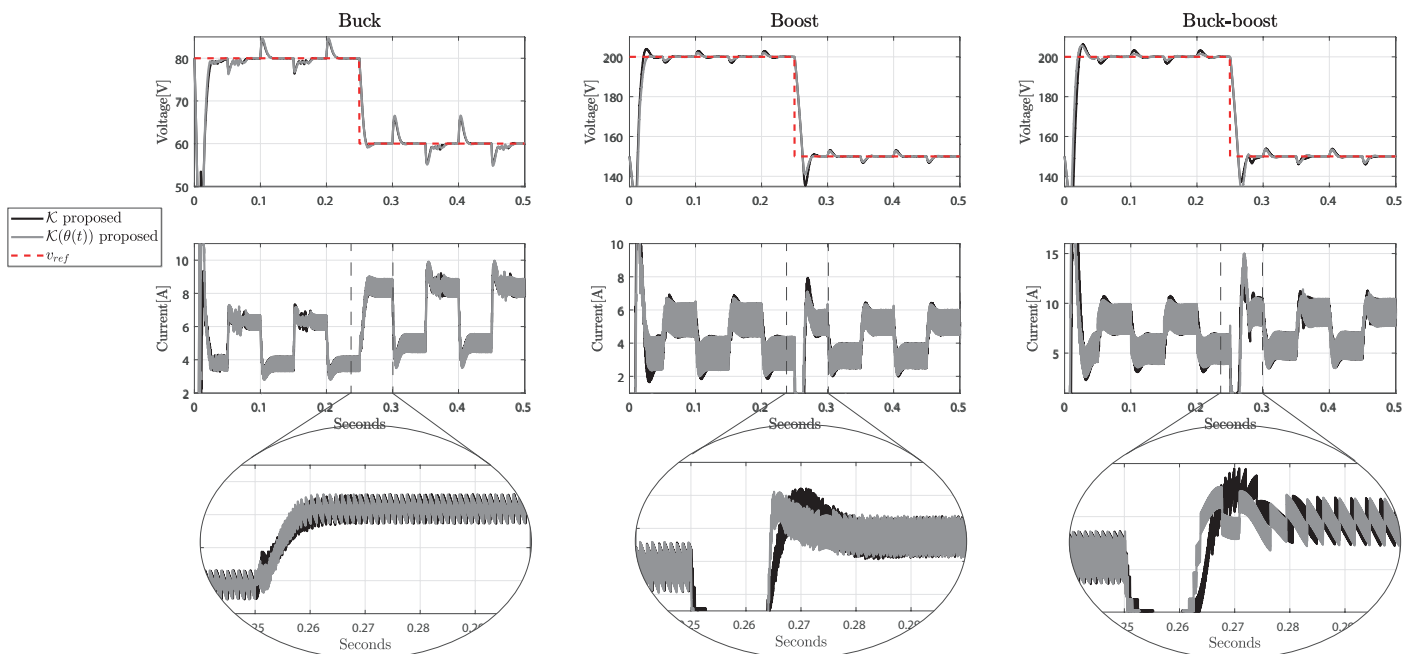


**Figure 10.** DC-DC converters states response for fixed and time-invariant case based on the CLP problem. This case considered the nominal value for  $V_{in} = 100$  V and  $P(t)$  as a square signal with amplitude  $\in [300\ 500]$  W and frequency of 10 Hz to simulate. The upper figures indicate the voltage and the setpoint on the three converters. The lower figures show the current obtained in the inductor. A zoom to the current plot is also presented.

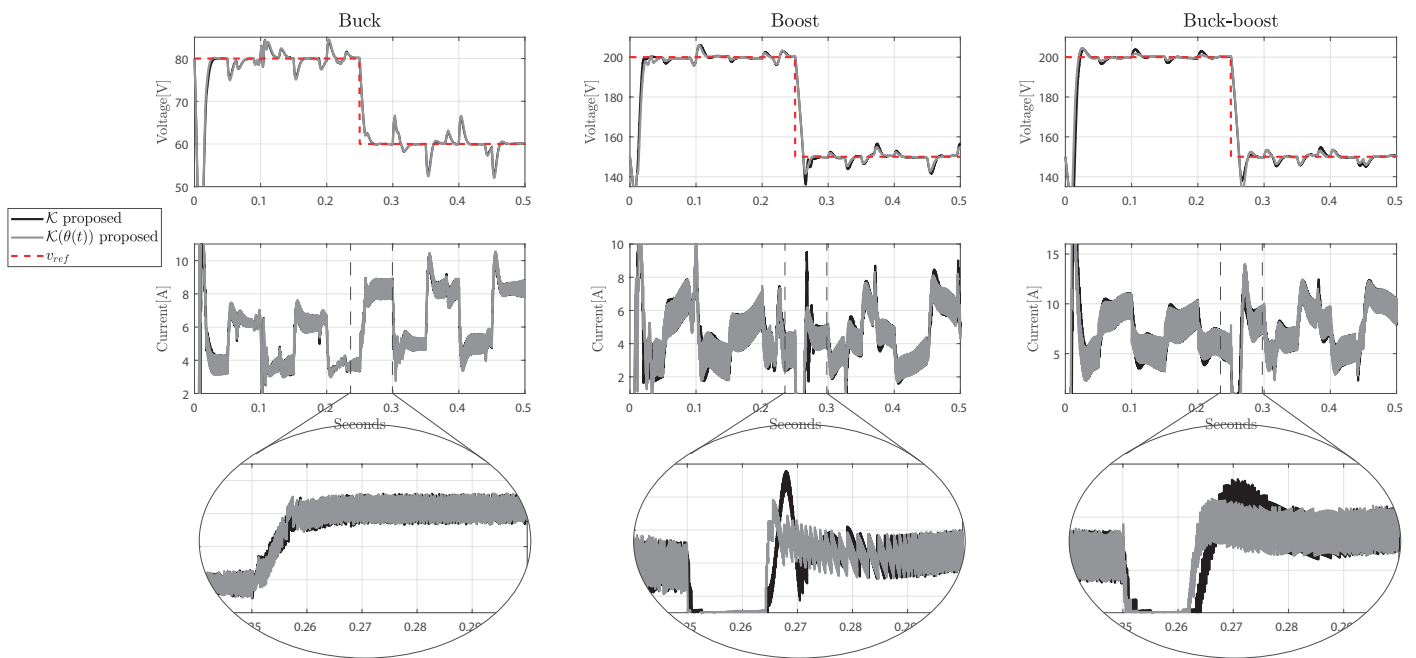


**Figure 11.** DC–DC converters state response for time-varying bounded case based on CLP problem assumed to vary according to:  $V_{in}(t) = 100 + 20\sin(50t)$  V and  $P(t)$  as a square signal with amplitude  $\in [300\ 500]$  W and frequency of 10 Hz. The upper figures indicate the voltage and the setpoint on the three converters. The lower figures show the current obtained in the inductor. A zoom to the current plot is also presented.

The proposed simulations show at a glance good performance provided by the designed controllers. When the demand of power changes, the voltage is affected generating a deviation with respect to the reference, which is  $4 V_{peak}$ ,  $7 V_{peak}$  and  $5 V_{peak}$  for buck, boost and buck-boost converter, respectively. These values represent a maximum variation of 5% with respect to the reference voltage in the worst case. Finally, the Appendix C presents a simulation evaluating the performance loss as a function of the sampling period when the proposed strategy is implemented in a digital controller.

### 7. Conclusions

A new LPV model-based methodology was proposed in this paper to address the problem of robust control of dc converters. The methodology was applied to the classic dc converters present in the literature, considering two scenarios: in PV source application (variations in input parameters) and CPL load (load-dependent dynamics). LMI conditions were employed to design gain-scheduled controllers that guarantee performance and stability. Thanks to the proposed controller structure, we were able to track a constant reference (commonly used in power converter systems). Note that in the Section 1, the state of the art for the design of static and dynamic controllers for the converter problems addressed in this paper was presented. However, techniques such as PID, and MPC [15,18] are designed under the assumption that the system is linear time-invariant and, consequently, cannot provide guarantees of stability and performance, especially in the presence of time-varying parameters, as in the cases investigated in this paper. As validation, two simulation cases were presented: the first showed the response for a fixed value of the parameters (to compare the dynamics performance under small variations of the operating point), and the second considered an extreme case where all parameters were assumed time-varying (inductor value, capacitor value, resistor, and voltage input with bounded time-varying values). The latter case is unrealistic, but it shows the robustness of the proposed controller, keeping the desired performance even in the worst-case scenario.

*Line of Research*

The next step of this research is to obtain gain-scheduled controllers for the CPL approach, adapt to a more complex microgrid and validate the simulation cases through experimental implementation.

**Author Contributions:** R.M.F. was primarily responsible for writing the article, supervised by J.M.P., H.G.J. and L.d.P.C. were responsible for the problem conceptualization. M.J.L. and A.J.R.—review and editing, and R.C.L.F.O. was the general supervisor of the work. All authors have read and agreed to the published version of the manuscript.

**Funding:** Chilean research agency ANID-fondecyt de iniciación grant 11201049, AC3E Basal Project FB0008. The Brazilian agency CNPq grant 315538/2021-0 and FAPESP grants 2015/02325-0 and 2020/16635-9.

**Institutional Review Board Statement:** Not applicable.

**Informed Consent Statement:** Not applicable.

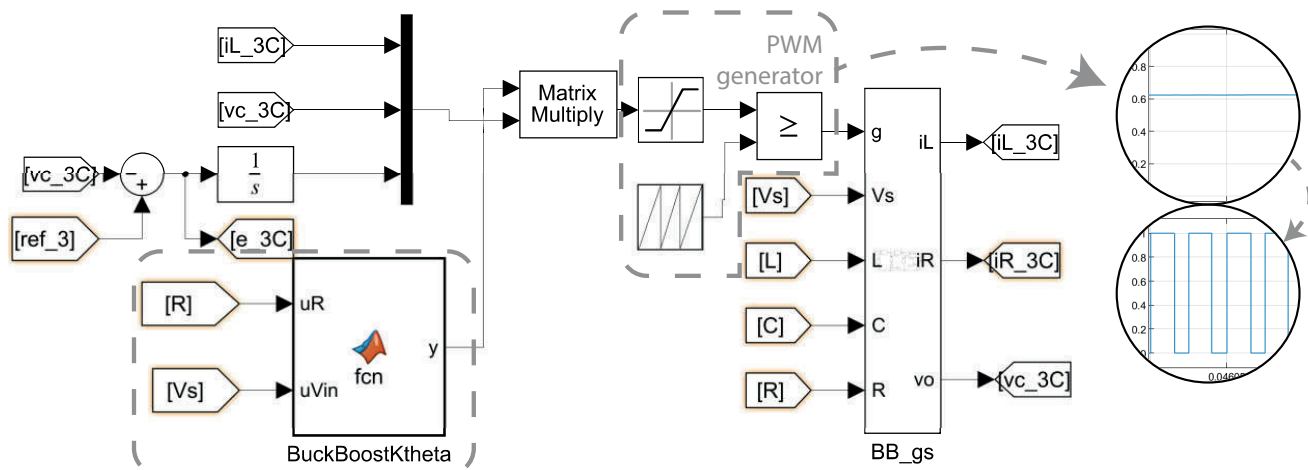
**Data Availability Statement:** Not applicable.

**Acknowledgments:** Acknowledgments to *Magister en Ciencias de la Ingeniería con mención en conversión de energía* program of the University of Talca, Chile; to Jorge A. Zolorza; and to Cecilia F. Morais for her contribution at the beginning of the work.

**Conflicts of Interest:** We declare no conflict of interest for all authors.

**Appendix A. Implementation in Electronic Specialized Software**

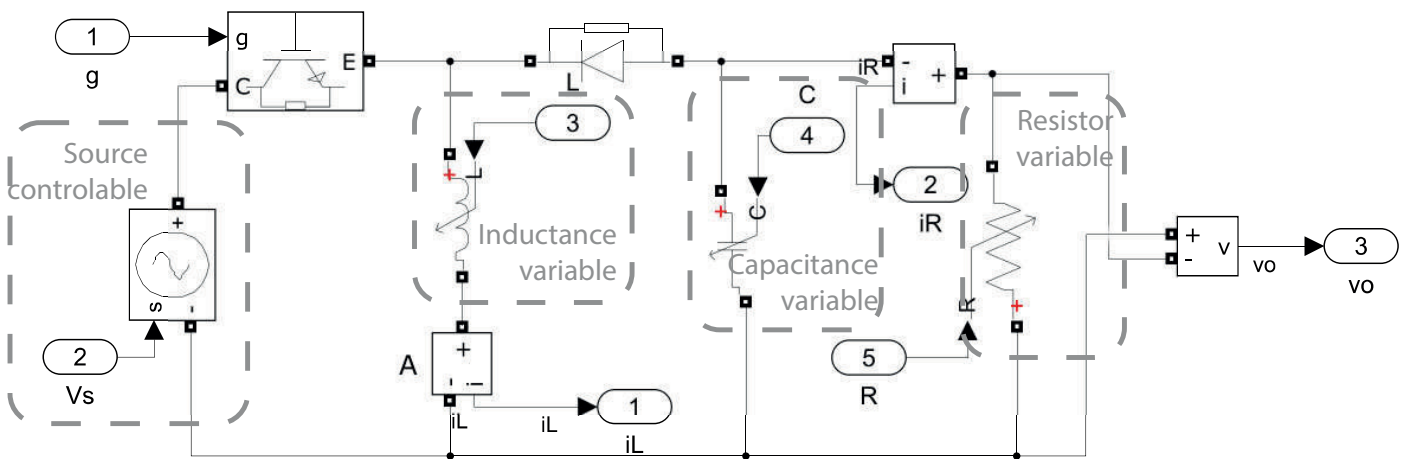
To hold the representativeness of a real system, specialized software was used. Figure A1 shows the workspace on *simulink* environment.



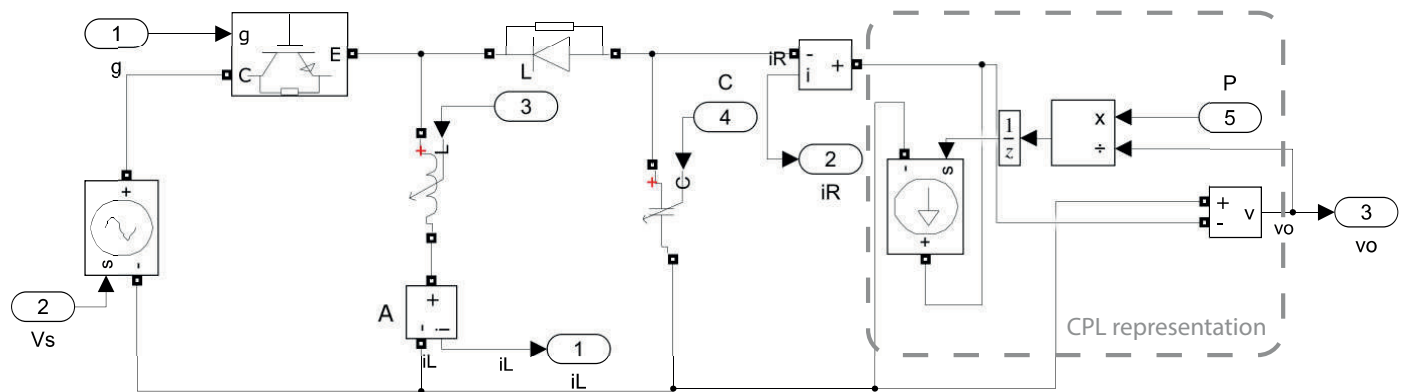
(a) The sub-system contains the electrical build of the buck-boost converter. A comparison is shown between a saturation signal and a triangular signal, which is the way to generate a PWM signal. The gain-scheduled controller is shown on the lower side.

**Figure A1.** *Cont.*





(b) This figure represent the inside of the sub-system. There are a voltage source, inductance, capacitance and resistor, all of which are variables. Their values are given by an arbitrary external signal.



(c) This figure represent the inside of the sub-system, but for the CPL case, which is shown at the right side. Their values are given by an arbitrary external signal.

**Figure A1.** The implementation on *simulink* is presented here: (a) Representation of buck-boost converter system build in a classic *simulink* environment block; (b) Buck-Boost electrical scheme build by a specialized block with  $R(t)$  load; (c) Buck-Boost electrical scheme build by a specialized block with CPL load. Note that the buck-boost converter can be replaced by another converter (electrical scheme).

### Appendix B. Computational Complexity

The computational framework used is the following: A personal computer equipped with CPU Ryzen 5600X stock frequency. 16 GB RAM DDR4 of 3000 MHz (2x8 GB). Windows 10 Pro (21H2 build) edition.

With respect to the LPV model, the most complex case corresponds to the boost-buck LVP model on the PV approach. This case has six parameter-dependent variables, yielding  $L = 2^6$  generated vertices in the polytopic model. The optimization problem has 10 SDP variables. The SDP solver takes 6.5 s to find a solution.

As for the online controller, Table A1 presents the number of operations performed at each control action update.

**Table A1.** Amount of operation to generate the control action online by  $\mathcal{K}(\theta(t))$  controller parameters.

Case	Converter	$n$ Time-Varying Parameter	Order	Operations	
				SUM	MULT
PV	buck	1	$A(\theta(t)) \in \mathcal{R}^{3 \times 3}$ $B(\theta(t)) \in \mathcal{R}^{3 \times 1}$	1	2
	boost	2		2	3
	buck-boost	2		2	3

**Appendix C. Performance Loss Concerning Sample Period**

A Zero-Order Holder (ZOH) was applied to the controller output to simulate digital control. The loss-index  $Q = \frac{\mathcal{J}(T)}{\mathcal{J}_c}$  was used to compare the performance loss through to a sweep in the sampling period of the ZOH.

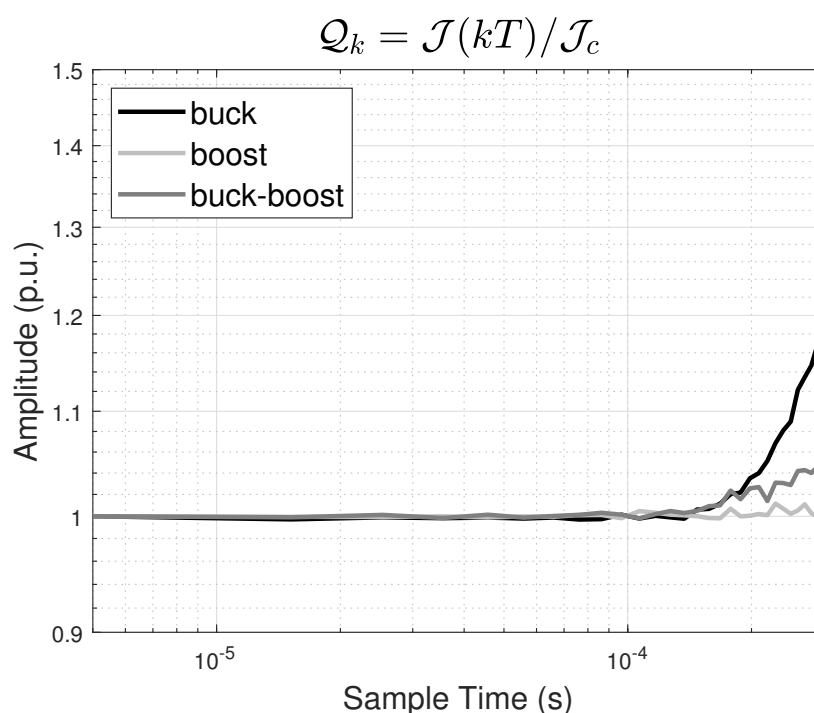


**Figure A2.** The value of  $Q$  is shown in *p.u.* as a function of the sampling period of a hypothetical microcontroller. The origin of the *x*-axis represents the system operating under a sampling period closed to 0 s (continuous-time), increasing this period to the right up to 0.3 ms.

**References**

- Aden, I.A.; Kahveci, H.; Şahin, M.E. Design and Implementation of Single-Input Multiple-Output DC–DC Buck Converter for Electric Vehicles. *J. Circuits Syst. Comput.* **2021**, *30*, 2150228. [CrossRef]
- Swaminathan, N.; Cao, Y. An Overview of High-Conversion High-Voltage DC–DC Converters for Electrified Aviation Power Distribution System. *IEEE Trans. Transp. Electrif.* **2020**, *6*, 1740–1754. [CrossRef]
- Ansari, S.; Chandel, A.; Tariq, M. A Comprehensive Review on Power Converters Control and Control Strategies of AC/DC Microgrid. *IEEE Access* **2021**, *9*, 17998–18015. [CrossRef]
- Baidya, S.; Potdar, V.; Pratim Ray, P.; Nandi, C. Reviewing the opportunities, challenges, and future directions for the digitalization of energy. *Energy Res. Soc. Sci.* **2021**, *81*, 102243. [CrossRef]
- Ullah, M.H.; Park, J.D. Distributed Energy Trading in Smart Grid Over Directed Communication Network. *IEEE Trans. Smart Grid* **2021**, *12*, 3669–3672. [CrossRef]
- Safayatullah, M.; Elrais, M.T.; Ghosh, S.; Rezaei, R.; Batarseh, I. A Comprehensive Review of Power Converter Topologies and Control Methods for Electric Vehicle Fast Charging Applications. *IEEE Access* **2022**, *10*, 40753–40793. [CrossRef]
- Kumar, K.R.; Raja, K.R.; Padmanaban, S.; Muyeen, S.M.; Khan, B. Comprehensive Review of KY Converter Topologies, Modulation and Control Approaches With Their Applications. *IEEE Access* **2022**, *10*, 20978–20994. [CrossRef]
- Anzalchi, A.; Sarwat, A. Overview of technical specifications for grid-connected photovoltaic systems. *Energy Convers. Manag.* **2017**, *152*, 312–327. [CrossRef]

9. Xu, J.; Gu, L.; Rivas-Davila, J. Effect of Class 2 Ceramic Capacitor Variations on Switched-Capacitor and Resonant Switched-Capacitor Converters. *IEEE J. Emerg. Sel. Top. Power Electron.* **2020**, *8*, 2268–2275. [CrossRef]
10. Deng, F.; Heng, Q.; Liu, C.; Wang, Q.; Zhu, R.; Cai, X.; Chen, Z. Power Losses Control for Modular Multilevel Converters Under Capacitor Deterioration. *IEEE J. Emerg. Sel. Top. Power Electron.* **2020**, *8*, 4318–4332. [CrossRef]
11. Schmitz, L.; Martins, D.C.; Coelho, R.F. Comprehensive Conception of High Step-Up DC–DC Converters With Coupled Inductor and Voltage Multipliers Techniques. *IEEE Trans. Circuits Syst. I Regul. Pap.* **2020**, *67*, 2140–2151. [CrossRef]
12. Zhou, S.; Mao, M.; Zhou, L.; Wan, Y.; Xi, X. A Shadow Fault Diagnosis Method Based on the Quantitative Analysis of Photovoltaic Output Prediction Error. *IEEE J. Photovolt.* **2020**, *10*, 1158–1165. [CrossRef]
13. Vu, V.B.; Tran, D.H.; Choi, W. Implementation of the Constant Current and Constant Voltage Charge of Inductive Power Transfer Systems With the Double-Sided LCC Compensation Topology for Electric Vehicle Battery Charge Applications. *IEEE Trans. Power Electron.* **2018**, *33*, 7398–7410. [CrossRef]
14. Arora, S.; Balsara, P.T.; Bhatia, D.K. Digital implementation of constant power load (CPL), active resistive load, constant current load and combinations. In Proceedings of the 2016 IEEE Dallas Circuits and Systems Conference (DCAS), Arlington, TX, USA, 10 October 2016; pp. 1–4. [CrossRef]
15. Verma, S.; Singh, S.K.; Rao, A.G. Overview of control Techniques for DC-DC converters. *Res. J. Eng. Sci.* **2013**, *2*, 18–21.
16. Rojas, D.; Muñoz, J.; Rivera, M.; Rothen, J. Review of Control Techniques in Microinverters. *Sensors* **2021**, *21*, 6486. [CrossRef]
17. Xu, Y.; Yang, Z.; Gu, W.; Li, M.; Deng, Z. Robust Real-Time Distributed Optimal Control Based Energy Management in a Smart Grid. *IEEE Trans. Smart Grid* **2017**, *8*, 1568–1579. [CrossRef]
18. Mumtaz, F.; Zaihar Yahaya, N.; Tanzim Meraj, S.; Singh, B.; Kannan, R.; Ibrahim, O. Review on non-isolated DC-DC converters and their control techniques for renewable energy applications. *Ain Shams Eng. J.* **2021**, *12*, 3747–3763. [CrossRef]
19. Boyd, S.; El Ghaoui, L.; Feron, E.; Balakrishnan, V. *Linear Matrix Inequalities in System and Control Theory*; Society for Industrial and Applied Mathematics: Philadelphia, PA, USA, 1994.
20. Aps, M. MOSEK Optimization Toolbox for MATLAB. In User’s Guide and Reference Manual. 2021. Available online: <http://docs.mosek.com/9.0/toolbox/index.html> (accessed on 1 August 2022).
21. Koch, G.G.; Maccari, L.A.; Oliveira, R.C.L.F.; Montagner, V.F. Robust  $H_\infty$  State Feedback Controllers Based on Linear Matrix Inequalities Applied to Grid-Connected Converters. *IEEE Trans. Ind. Electron.* **2019**, *66*, 6021–6031. [CrossRef]
22. Li, Z.; Zang, C.; Zeng, P.; Yu, H.; Li, S.; Bian, J. Control of a Grid-Forming Inverter Based on Sliding-Mode and Mixed  $H_2/H_\infty$  Control. *IEEE Trans. Ind. Electron.* **2017**, *64*, 3862–3872. [CrossRef]
23. Mardani, M.M.; Vafamand, N.; Khooban, M.H.; Dragičević, T.; Blaabjerg, F. Design of Quadratic D-Stable Fuzzy Controller for DC Microgrids With Multiple CPLs. *IEEE Trans. Ind. Electron.* **2019**, *66*, 4805–4812. [CrossRef]
24. Xiong, P.; Wang, F.; Cao, X.; Duan, G. Robust D-stability LMI conditions of matrix polytopes via affine parameter-dependent Lyapunov functions. *J. Syst. Eng. Electron.* **2013**, *24*, 984–991. [CrossRef]
25. Torres-Pinzón, C.A.; Paredes-Madrid, L.; Flores-Bahamonde, F.; Ramirez-Murillo, H. LMI-Fuzzy Control Design for Non-Minimum-Phase DC-DC Converters: An Application for Output Regulation. *Appl. Sci.* **2021**, *11*, 2286. [CrossRef]
26. Ramirez, H.; Garzón, G.; Torres, C.; Navarrete, J.; Restrepo, C. LMI Control Design of a Non-Inverting Buck-Boost Converter: A Current Regulation Approach. *Tecciencia* **2017**, *12*, 79–85. [CrossRef]
27. Paez, J.D.; Frey, D.; Maneiro, J.; Bacha, S.; Dworakowski, P. Overview of DC-DC Converters Dedicated to HVdc Grids. *IEEE Trans. Power Deliv.* **2019**, *34*, 119–128. [CrossRef]
28. Gorji, S.A.; Sahebi, H.G.; Ektesabi, M.; Rad, A.B. Topologies and control schemes of bidirectional DC–DC power converters: An overview. *IEEE Access* **2019**, *7*, 117997–118019. [CrossRef]
29. Azer, P.; Emadi, A. Generalized state space average model for multi-phase interleaved buck, boost and buck-boost DC-DC converters: Transient, steady-state and switching dynamics. *IEEE Access* **2020**, *8*, 77735–77745. [CrossRef]
30. Gamoudi, R.; Elhak Chariag, D.; Sbita, L. A Review of Spread-Spectrum-Based PWM Techniques—A Novel Fast Digital Implementation. *IEEE Trans. Power Electron.* **2018**, *33*, 10292–10307. [CrossRef]
31. Cuk, S.; Middlebrook, R. A general unified approach to modelling switching DC-to-DC converters in discontinuous conduction mode. In Proceedings of the 1977 IEEE Power Electronics Specialists Conference, Palo Alto, CA, USA, 14–16 June 1977; pp. 36–57.
32. Middlebrook, R.D.; Cuk, S. A general unified approach to modelling switching-converter power stages. In Proceedings of the 1976 IEEE Power Electronics Specialists Conference, Cleveland, OH, USA, 8–10 June 1976; pp. 18–34.
33. Liang, T.J.; Chen, K.H.; Chen, J.F. Primary Side Control For Flyback Converter Operating in DCM and CCM. *IEEE Trans. Power Electron.* **2018**, *33*, 3604–3612. [CrossRef]
34. Torres-Pinzón, C.A.; Giral, R.; Leyva, R. LMI-based robust controllers for DC-DC cascade boost converters. *J. Power Electron.* **2012**, *12*, 538–547. [CrossRef]
35. Gkizas, G. Optimal robust control of a Cascaded DC–DC boost converter. *Control Eng. Pract.* **2021**, *107*, 104700. [CrossRef]
36. Agulhari, C.M.; Felipe, A.; Oliveira, R.C.L.F.; Peres, P.L.D. Algorithm 998: The Robust LMI Parser—A toolbox to construct LMI conditions for uncertain systems. *ACM Trans. Math. Softw.* **2019**, *45*, 36:1–36:25. Available online: <http://rolmip.github.io> (accessed on 2 August 2022). [CrossRef]
37. Explorador Solar—Ministerio de Energia. Available online: <https://solar.minenergia.cl/exploracion> (accessed on 1 March 2022).
38. The MathWorks, I. Simscape/Specialized Power Systems Toolbox, Natick, Massachusetts, United States. 2022. Available online: <https://www.mathworks.com/products/simscape.html> (accessed on 2 August 2022)

39. Packard, A.; Poolla, K.; Horowitz, R. Jacobian Linearizations, Equilibrium Points. In *Dynamic Systems and Feedback*; Prentice Hall: Berkeley CA, USA, 2002.
40. Zolorza, J.A.; Palma, J.M.; Carvalho, L.P.; Bustos, D.; Morais, C.F.; Barbosa, K.A. Multi-Equilibrium Point Coupled Tanks System: A tutorial about LPV modelling and control design. In Proceedings of the 2021 IEEE CHILEAN Conference on Electrical, Electronics Engineering, Information and Communication Technologies (CHILECON), Valparaíso, Chile, 6–9 December 2021; pp. 1–7. [[CrossRef](#)]
41. Apte, A.; Joshi, V.A.; Mehta, H.; Walambe, R. Disturbance-Observer-Based Sensorless Control of PMSM Using Integral State Feedback Controller. *IEEE Trans. Power Electron.* **2020**, *35*, 6082–6090. [[CrossRef](#)]